PROTEINS
STRUCTURE ■ FUNCTION ■ BIOINFORMATICS

Insights on the acetylated NF-κB transcription factor complex with DNA from molecular dynamics simulations

Cristina Fenollar-Ferrer,[1*] Claudio Anselmi,[1] Vincenzo Carnevale,[2] Simone Raugei,[3] and Paolo Carloni[4]

[1] Max Planck Institute of Biophysics, Frankfurt am Main, Germany
[2] Institute for Computational Molecular Science, Temple University, Philadelphia, Pennsylvania
[3] Pacific Northwest National Laboratory, Richland, Washington
[4] German Research School for Simulation Science, Jülich Research Center and RWTH, University of Aachen, Germany

ABSTRACT

The nuclear factor-κB (NF-κB) is a DNA sequence-specific regulator of many important biological processes, whose activity is modulated by enzymatic acetylation. In one of the best functionally characterized NF-κB complexes, the p50/p65 heterodimer, acetylation of K221 at p65 causes a decrease of DNA dissociation rate, whilst the acetylation of K122 and K123, also at p65, markedly decreases the binding affinity for DNA. By means of molecular dynamics simulations based on the X-ray structure of the p50/p65 complex with DNA, we provide insights on the structural determinants of the acetylated complexes in aqueous solution. Lysine acetylation involves the loss of favorable electrostatic interactions between DNA and NF-κB, which is partially compensated by the reduction of the desolvation free-energy of the two binding partners. Acetylation at both positions K122 and K123 is associated with a decrease of the electrostatic potential at the p65/DNA interface, which is only partially counterbalanced by an increase of the local Na^+ concentration. It induces the disruption of base-specific and nonspecific interactions between DNA and NF-κB and it is consistent with the observed decrease of binding affinity. In contrast, acetylation at position K221 results in the loss of nonspecific protein–DNA interactions, but the DNA recognition sites are not affected. In addition, the loss of protein–DNA interactions is likely to be counterbalanced by an increase of the configurational entropy of the complex, which provides, at a speculative level, a justification for the observed decrease of NF-κB/DNA dissociation rate.

Proteins 2012; 80:1560–1568.

Key words: transcription factor; MD; lysine acetylation; DNA binding affinity; post-translational modifications; transcription regulation.

INTRODUCTION

The nuclear factor-κB/Rel (NF-κB/Rel) is one of the most intensively studied families of DNA sequence-specific transcription factors. It is constituted by homodimer or heterodimer featuring the ubiquitous Rel homology domain (RHD), which shares 35–61% sequence identity across the family.[1–3] Rel members include p50 (NF-κB1), p52 (NF-κB2), c-Rel, p65 (RelA), and RelB.[4] The heterodimer p50/p65 is the most abundant. These proteins regulate a wide variety of processes activated under stress-related signals as immune, inflammatory and anti-apoptotic responses, cellular growth and development.[4–6] Misregulation of these transcription factors is associated with a wide variety of diseases including acute inflammatory reactions, atherosclerosis, neurodegenerative diseases, viral infections of the central nervous system and tumors.[2,7–12] Therefore, the NF-κB/Rel family is a promising pharmacological target for many pathologies.[13–16]

NF-κB activity in the cell is controlled at two levels: activation and regulation. The activation process is performed in the cytoplasm, where NF-κB is bound to the inhibitory IκB protein. During activation, IκB is phosphorylated, ubiquitinated, and finally degradated, causing NF-κB to diffuse to the nucleus, where it activates transcription of specific target genes.[4]

The transcription of the NF-κB-activated genes is regulated (i.e., enhanced, decreased, or stopped) by other DNA-binding proteins, transcription factors and enzymes. Acetylation of NF-κB constitutes an important direct mechanism of regulation of the transcription factor activity.[17,18] It is controlled by specific histone acetyltransferases (such as CBP/p300 and PCAF),[6] and

Additional Supporting Information may be found in the online version of this article.
Abbreviations: HDAC, histone deacetylase; MD, molecular dynamics; MM, molecular mechanics; NF, nuclear factor; PBSA, Poisson Boltzmann surface area; RHD, Rel homology

Cristina Fenollar-Ferrer and Claudio Anselmi contributed equally to this work.
*Correspondence to: C. Fenollar Ferrer; Max-Planck-Institut für Biophysik, Max-von-Laue-Straße 3, 60438 Frankfurt am Main, Germany. E-mail: cristina.fenollar-ferrer@biophys.mpg.de.
Received 23 September 2011; Revised 15 January 2012; Accepted 25 January 2012
Published online 6 February 2012 in Wiley Online Library (wileyonlinelibrary.com).
DOI: 10.1002/prot.24047

turned off by specific histone deacetylases (HDACs) (such as HDAC3).[5,6,17,19–26]

The process affects DNA binding affinity in a subtle way. In the case of NF-κB p50/p65 bound to a κB enhancer oligonucleotide, acetylation of K221 causes a decrease of the complex dissociation rate,[18,27] whilst acetylation of K122 and K123 causes a significant decrease of NF-κB affinity for DNA.[17,18]

From the crystal structure of the nonacetylated p50/p65 complex with DNA, it emerges that the three lysines involved in the acetylation process form similar, nonspecific interactions with DNA.[28] However, the structural determinants of the acetylated complexes are not known. So far, it has been suggested that acetylation at K221 causes conformational changes of the protein.[17] Here, we address this issue by performing molecular dynamics (MD) simulations on the nonacetylated, monoacetylated, at K221, and diacetylated, at K122 and K123, NF-κB/DNA complexes in aqueous solution at room temperature and pressure, based on the available structural information.[28] The comparison of the MD trajectories casts light onto the mechanism by which lysine acetylation regulates DNA affinity of NF-κB.

METHODS

The initial model of the nonacetylated complex was taken from the crystal structure of murine NF-κB p50/p65 heterodimer in complex with immunoglobulin κB DNA (PDB entry: 1VKX).[28]

The structure was inserted in a box of edges ~88 × 106 × 120Å filled with ~33,800 TIP3P water molecules.[29] 22 Na^+ counterions were also necessary for the electroneutrality. The total system consisted of ~111,400 atoms.

After the acetylation of the lysines and minimization (see Supporting Information), 60-ns unrestrained MD simulations were carried out for the three systems. The adopted force field for all the simulations was the AMBER parm99 force field.[30,31] Atom point charges of the acetylated lysines were calculated by means of *ab initio* calculations after geometry optimization at HF/6-31G(d) level, by using the Gaussian03 program (Gaussian, Wallingford, CT), and RESP fitting.[32] MD simulations were performed using the Gromacs 3.3.1 package.[33,34]

Trajectory analyses were performed for the last 20 ns of the trajectories by using the available tools in Gromacs[33,34] and the VMD 1.8.6 program.[35] The latter was also used for molecular visualization. DNA helical parameters were calculated by using the Curves 5.3 program.[36] DNA curvature was evaluated following the study by Anselmi et al.[37] Definitions and nomenclature of DNA structural components can be found in the reference.[38] Poisson-Boltzmann electrostatic potential at the protein surface was calculated by means of APBS 0.5.1 program.[39] Molecular mechanics/Poisson Boltzmann surface area (MM/PBSA) calculations[40] were performed by using the relative tool in the AmberTools package.[41]

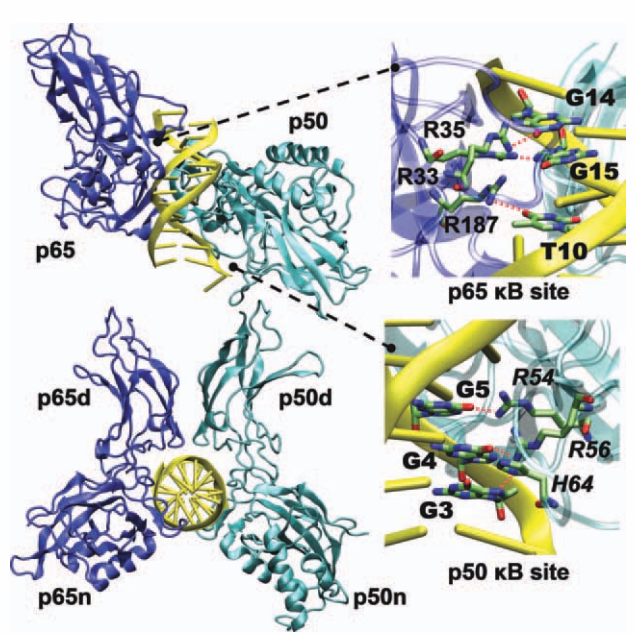

Figure 1

Structure of the complex between the p50/p65 heterodimer and the immunoglobulin κB DNA with sequence 5′-TGGGGACTTTCC-3′/5′-AGGAAAGTCCCC-3′. Each of the subunits is formed by the so-called dimerization domain (p50d and p65d) and the N-terminal domain (p50n and p65n). The DNA duplex (yellow ribbon) interacts with the loops from the edges of the N- and C-terminal domains of p50 (cyan ribbon) and p65 (blue ribbon): 5′-GGGAC-3′/5′-GTCCC-3′ is recognized by p50 and 5′-TTCC-3′/5′-GGAA-3′ by p65. p50 forms sequence-specific hydrogen bonds between *R54* and **G5**, *R56* and **G4**, *H64* and **G3**, *K241*, and **G19**. p65 binds to DNA by forming hydrogen bonds between R33 and **G15**, R35, and **G14**, R187, and **T10**.

RESULTS AND DISCUSSION

In the crystal structure of NF–κB p50/p65 complex with immunoglobin κB DNA (Fig. 1), each RHD is formed by two domains connected by a flexible linker. The dimer occurs at the so-called C-terminal dimerization domains, generally referred to as p50d and p65d, respectively. The N-terminal domains are generally referred to as p50n and p65n, respectively. The DNA contacts with the protein are mediated by the loops from the edges of the N- and C-terminal domains of p50 and p65. DNA recognition by NF-κB occurs at two specific κB subsites[4] through the formation of H-bonds involving residues R187, R35, and R33 of p65, *R54*, *R56*, *H64*, and *K241* of p50 and DNA bases **G3**, **G4**, **G5**, **T10**, **G14**, **G15**, and **G19** (Fig. 1). Hereafter, residues belonging to p50 subunit are written in italics throughout the text, while DNA bases are indicated in bold. The H-bonding interactions mentioned above are referred as specific

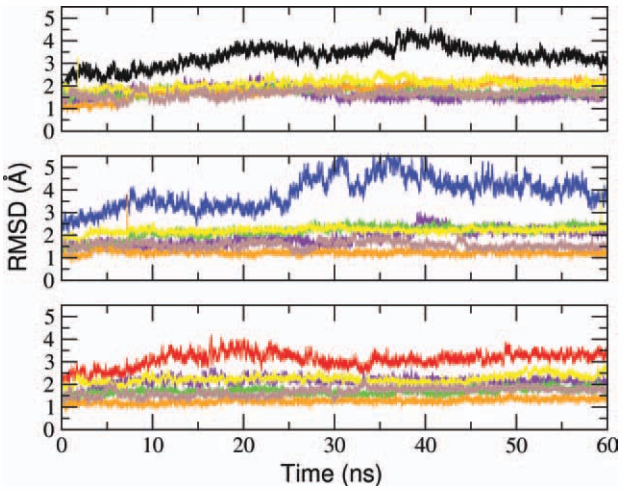

Figure 2

RMSD of the complexes investigated here as a function of the simulated time. Black, blue, and red lines represent the total RMSD of 0AC, 1AC, and 2AC, respectively, as a function of time. RMSD of the DNA (violet) and the different protein domains are also reported (p65n: green; p65d: orange; p50n: yellow; p50d: brown). [Color figure can be viewed in the online issue, which is available at wileyonlinelibrary.com.]

interactions to differentiate them from all the other protein–DNA contacts (nonspecific interactions).

In the following, we discuss the results from a series of 60-ns MD simulations of nonacetylated, monoacetylated, and diacetylated complexes (hereafter 0AC, 1AC, and 2AC, respectively).

0AC

To validate our computational approach, we have first chosen a number of properties to compare the structural ensemble resulting from the trajectory of our model system (0AC) with the crystal structure. The adopted structural parameters vary from quantitative geometrical descriptors (e.g., RMSD, BI/BII DNA backbone transitions,[42] DNA curvature, and inter- and base-base parameters) to a qualitative analysis of the specific and nonspecific protein/DNA interactions.

The RMSD reaches a plateau after ~20 ns at ~3.5Å from the X-ray structure (Fig. 2). Instead, the RMSD of the DNA and each single protein domain is markedly smaller reaching at most a value of ~2Å; therefore, these values exclude major conformational changes within the domains and point to the role of relative movements of the different subunits in generating structural heterogeneity.

BI/BII conformations are conserved along the trajectory (Fig. 3), except for **A16**.

The calculated DNA axis bend (16.0° ± 8.3°, Fig. 4) is similar to that of the initial X-ray structure.[28] It is also consistent with biochemical experiments, which point to a value ranging between 14° and 17°.[43]

Inter- and base-base parameters are very similar to the crystal structure and are close to the values expected for the canonical B-DNA conformation (Fig. 5). Some of the bases at the κB sites recognized by K122, K123, and K221, (e.g., **T10/A16**, **G3/C23**, and **G4/C22**) show the largest deviations. K122 and K123 are, actually, significantly closer to the DNA phosphate moieties than in the crystal structure. In fact, the distances measured from the X-ray conformation are more similar to the ones observed for 2AC, where the charges on the lysines have been vanished (Supporting Information Fig. S1A). Furthermore, the buried interface area upon complex formation in 0AC is slightly higher than in the crystal structure (Fig. 6), supporting the notion that the 0AC complex is

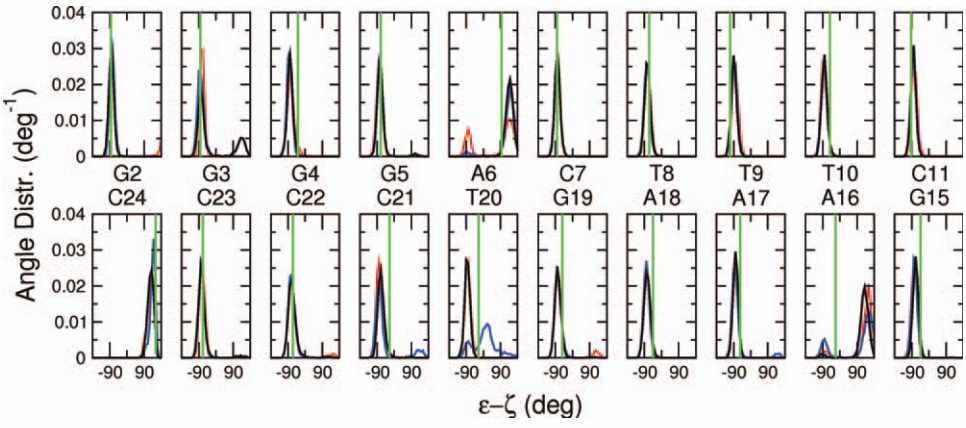

Figure 3

DNA BI/BII conformations. Normalized distributions are plotted for 0AC (black), 1AC (blue), and 2AC (red). The green lines indicate the values in the crystallographic structure. The DNA backbone dihedral angles ϵ and ζ (see Supporting Information Chart S1 for their definition) identifies the DNA conformation. The difference between the two angles (ϵ-ζ) is negative in BI and positive in BII.[42] [Color figure can be viewed in the online issue, which is available at wileyonlinelibrary.com.]

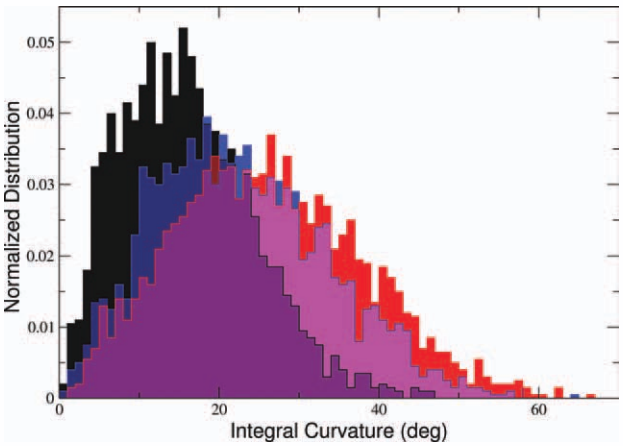

Figure 4

Normalized curvature distribution of the central eleven base pairs of the κB DNA. Black represents 0AC, blue represents 1AC, and red represents 2AC. Purple corresponds to superimposition of blue and red graph areas (1AC and 2AC). Darker colors represent superimpositions of the graph area with the black one (0AC). [Color figure can be viewed in the online issue, which is available at wileyonlinelibrary.com.]

more tightly bound than the X-ray structure. From the crystal structure, one may infer that K122 and K123 form salt bridges with D125 and D151, respectively (Supporting Information Fig. S1A); therefore, we have also monitored the distances between these residues during the simulations. Interestingly, the K122–D125 and K123–D151 distances are maintained in 2AC, whilst they are larger in 0AC and 1AC (Supporting Information Fig. S1A). These discrepancies can be attributed to several factors. These include the fact that our system is simulated in aqueous solution and, therefore, interactions resulting from packing effects in the X-ray structure are absent, as well as the different ionic strengths between our simulation setup and the crystallization buffer. However, these differences do not entail any structural rearrangement of p65n as the relative positions of K122, K123, and D125, D151 are very similar in all the simulations (Supporting Information Fig. S1B).

Base-specific H-bonds between the κB subsites and p50/p65 are all maintained during the simulation (Fig. 7, Supporting Information Table S1).[28]

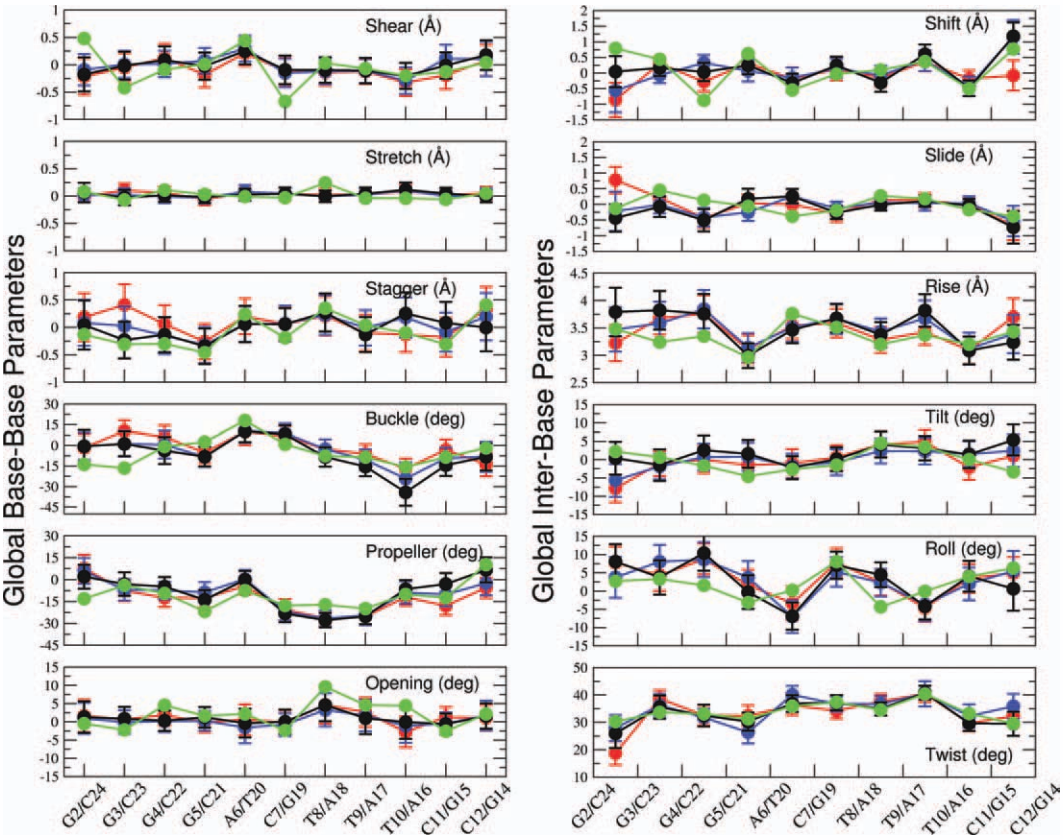

Figure 5

Global DNA inter- and base-base geometrical parameters as a function of DNA sequence position. Color coding as in Figure 3. The parameters are reported as average ± standard deviation. [Color figure can be viewed in the online issue, which is available at wileyonlinelibrary.com.]

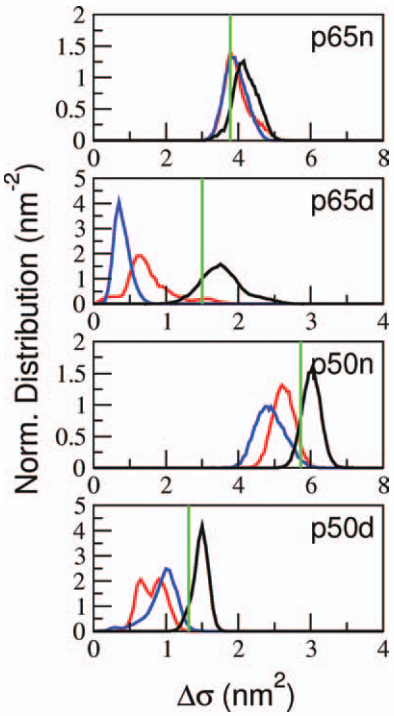

Figure 6

Distribution of the buried interface area between the DNA and the four protein subunits. These values have been chosen as representative of the amount of nonspecific interactions among DNA and NF-κB. Color coding as in Figure 3. [Color figure can be viewed in the online issue, which is available at wileyonlinelibrary.com.]

Despite minor structural details, our approach is capable of describing the most important feature of the nonacetylated NF-κB/DNA complex, that is, the structure of the DNA is accurately preserved. Indeed, even though the force field adopted in this study (AMBER parm99)[30,31] has been observed to cause distortions of the geometry of DNA beyond 50 ns,[44] no distortions were observed here, possibly because DNA is bound to a protein.

1AC

For this complex, we have repeated the same analyses done for 0AC. Despite the total RMSD values are quite high (∼4Å), the RMSD of the single domains is always ∼2Å or lower (Fig. 2). As for the case of AC0, these values suggest that monitoring the relative movements of the different domains is crucial to describe the structural ensemble.

Acetylation at K221 leads to the decrease of nonspecific interactions between DNA and NF-κB (Fig. 6), causing the detachment of p65d from the DNA (Supporting Information Fig. S2). The DNA bending is on average higher than in 0AC (23° ± 11°). Furthermore, highly bent configurations are more populated than in 0AC (Fig. 4).

In contrast, DNA/protein specific interactions are maintained except for R187 (which loses its H-bond interactions with **T10**) and for *K241* (which interacts with **A6** rather than with **G19**) (Fig. 7). Possibly because

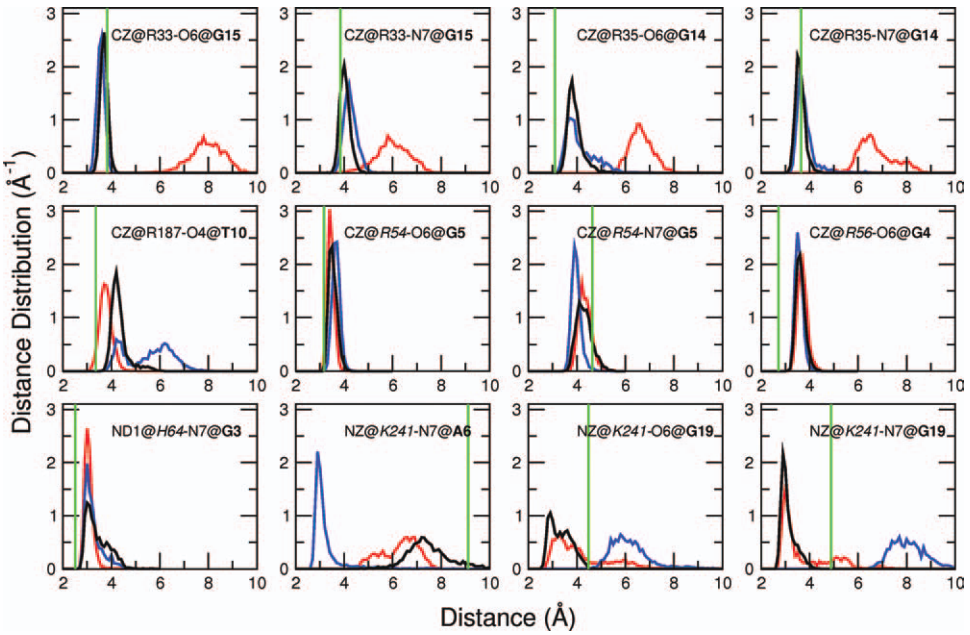

Figure 7

Specific p50 and p65 contacts with DNA. Distances between H-bond donors and acceptors are reported as normalized distributions. Color coding as in Figure 3. [Color figure can be viewed in the online issue, which is available at wileyonlinelibrary.com.]

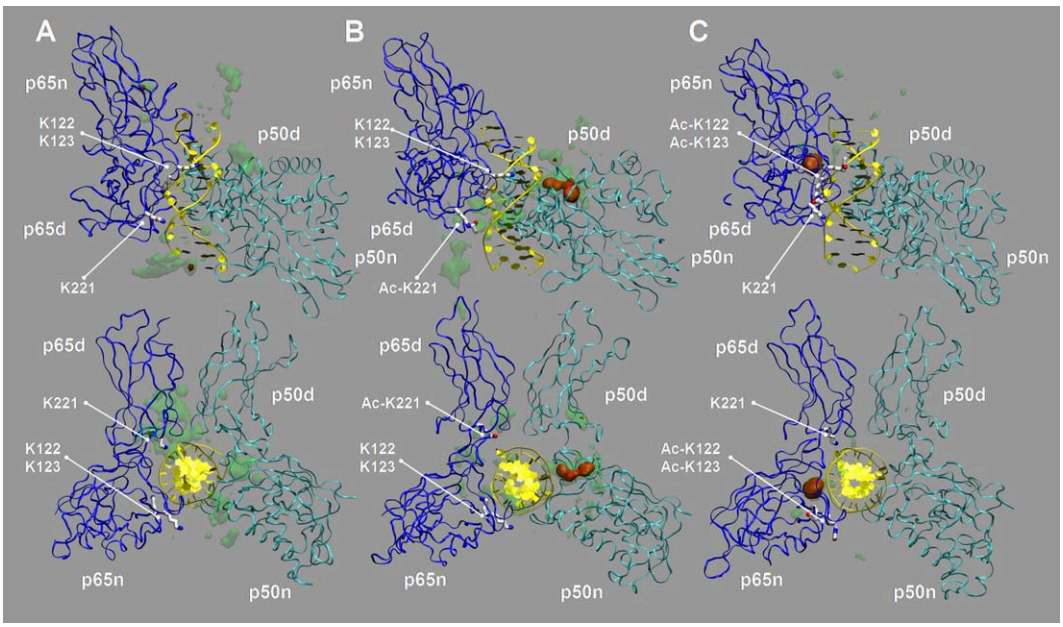

Figure 8

Average distribution of Na^+ counterions at the NF-κB/DNA surface (**A**) 0AC; (**B**) 1AC; (**C**): 2AC. p50 and p65 subunits are represented as cyan and blue ribbons, respectively; lysines 122, 123, and 221 in their nonacetylated or acetylated forms are in licorice representation. DNA is represented as yellow ribbons. Na^+ ion density is represented as isosurfaces. [Color figure can be viewed in the online issue, which is available at wileyonlinelibrary.com.]

of these rearrangements, we observe the backbone conformational change of **T20**, which is the base facing **A6** (Fig. 3), while the values of the rise and buckle at **T10**/**A16** base pair get slightly closer to those of canonical B-DNA (Fig. 5).

2AC

Analogously to 0AC and 1AC, the RMSD points out the relative movements of the different subunits.

As expected, Ac-K122 and Ac-K123 side chains are not in contact with the DNA backbone (Supporting Information Fig. S1A). The most dramatic effect is the loss of all of the base-specific interactions involving p65, but that of R187 with **T10** (Fig. 7), and Na^+ ions accumulate at the p65/DNA interface (Fig. 8). On average, one cation is found in the electrostatic "cavity" created at the binding sites. This suggests that the diacetylation reduces the ability of p65 subunit of counteracting the negative potential arising from DNA backbone. This is further confirmed by the

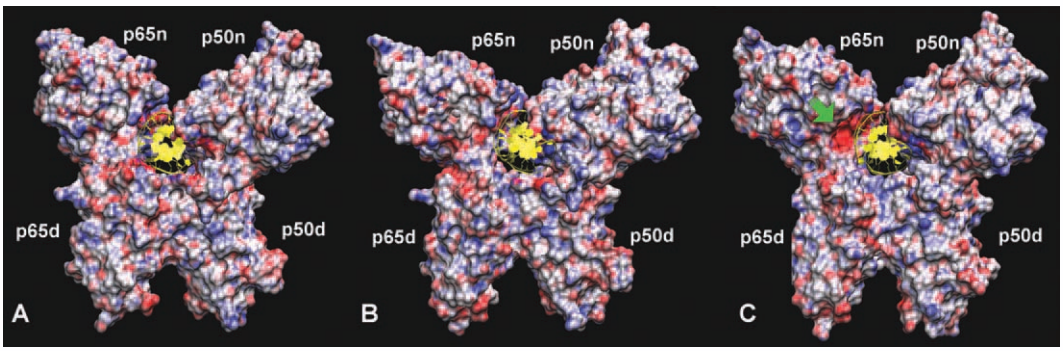

Figure 9

Electrostatic potential at NF-κB/DNA surface (**A**) 0AC; (**B**) 1AC; (**C**) 2AC. The protein is represented as contact surface; DNA is represented as yellow ribbons. Color scale ranges from -8 k_bT/e (red) to +8 k_bT/e (blue). In C, the green arrow indicates the region with largest decrease in electrostatic potential. [Color figure can be viewed in the online issue, which is available at wileyonlinelibrary.com.]

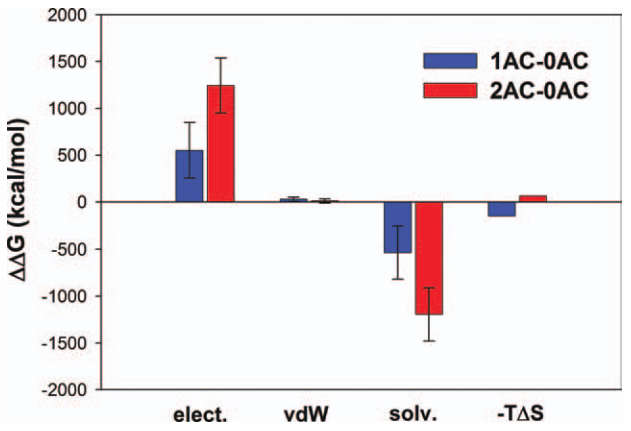

Figure 10

Relative contribution to the DNA binding free energy for 1AC and 2AC with respect to 0AC. Electrostatic, van der Waals, and solvation terms has been calculated in the framework of the MM/PBSA method.[40] Values are reported as average ± standard deviation. The entropy contributions have been calculated according to Schlitter.[45] [Color figure can be viewed in the online issue, which is available at wileyonlinelibrary.com.]

calculation of the electrostatic potential at the complex surface, which shows a much more negative and larger cavity on p65 subunit near the acetylated lysines (Fig. 9).

Nonspecific interactions between DNA and both dimerization domains are also largely reduced (Fig. 6), as shown also by the increased distances between DNA and p50d, p65d (Fig. S2).

The DNA bending is larger than that in 0AC and 1AC ($26^\circ \pm 12^\circ$) (Fig. 4). Similarly to 1AC, this reflects the weaker interactions between DNA and the proteins with respect to 0AC.

BI/BII conformations are maintained, except for **A6**, which shows equilibrium between the two conformations (Fig. 3).

Despite the loss of the specific interactions between p65n and DNA, no significant changes in the DNA nonspecific interactions with p65n, as well as the DNA specific and nonspecific interactions with p50n (Figs. 6 and 7) were observed, suggesting that specific interactions between p65n and DNA play a major role in stabilizing the complex.

To gain insights about the free energy associated with the structural changes on acetylation, we have performed MM/PBSA calculations.[40] In this method, a representative ensemble of conformations is used to calculate the free energy change between two states (typically a bound and free state of two interacting molecules). Free-energy differences are calculated by combining the so-called gas phase energy contributions as well as solvation free-energy components calculated from an implicit solvent model. These calculations suggest that, on the one hand, acetylation strongly destabilizes 1AC and, to a larger extent, 2AC relative to 0AC by increasing the electrostatic protein–DNA interaction energy (Fig. 10). On the other hand, it favors the desolvation of the binding partners and, consequently, the formation of 1AC and 2AC relative to 0AC. Despite these energy differences are very high, they counterbalance each other. The other contributions, for example, van der Waals interactions, turn out to have much smaller differences. Eventually, in the framework of the MM/PBSA methods, the binding free energy of the 1AC and 2AC complexes result to be less favorable than 0AC by ~44 kcal/mol and ~60 kcal/mol, respectively.

MM/PBSA calculations, however, do not take into account the crucial conformational entropy contribution to the free energy. An upper bound of such contribution has been calculated here using the formula introduced by Schlitter.[45] 1AC turns out to show larger fluctuations with respect to 0AC and 2AC (Supporting Information Fig. S3). This is translated into higher conformational entropy for the 1AC complex, whereas the 2AC complex has the lowest.

At the speculative level, these highly approximate calculations allow us to put forward the hypothesis that 1AC gains additional stabilization free energy with respect to 0AC because of the larger configurational entropy, which may compensate for the changes in other contributions, as it results from the MM/PBSA methods. In contrast, the 2AC complex results to be destabilized with respect to 0AC by both MM/PBSA and entropy contributions.

CONCLUSIONS

NF-κB p50/p65 acetylation modulates its DNA binding affinity, nuclear export, assembly with inhibitor and, eventually, the expression of NF-κB-induced genes.[23] However, the structural changes associated with acetylation have been not characterized so far. Here we have compared MD simulations of the nonacetylated (0AC), the monoacetylated (1AC), and the diacetylated (2AC) complexes.

In the case of acetylation at K122 and K123, specific and nonspecific contacts between NF-κB and the DNA are lost, or significantly weaker. The lack of positive charges at the lysine positions strongly increases both the negative electrostatic potential and Na^+ counterions density at the p65/DNA interface. This is confirmed by the energetic calculations, which show a destabilization of the diacetylated complex. As a whole, these results are consistent with the experimental evidence that acetylation at K122 and K123 strongly reduces the NF-κB affinity for its cognate DNA.[6,17,18,23,26]

In contrast, the effect of acetylation at K221 has been shown to decrease the dissociation rate of DNA compared with the nonacetylated complex,[18,27] suggesting that the loss of favorable electrostatic interactions should be compensated by other effects.

Our simulations show that the salt-bridge involving K221 in 0AC is responsible for a tight association between NF-κB and DNA. Acetylation at this lysine weakens the interactions between DNA and both p65d and p50, while leaving the interactions between DNA and p65n unaffected. However, these changes also result into a more favorable solvation, highest conformational flexibility, and a slight structural relaxation of the DNA molecule.

At a speculative level, we expect these effects to provide a net stabilization of 1AC compared with 0AC thereby explaining the observed decrease of DNA dissociation rate.[18,27]

ACKNOWLEDGMENTS

The authors thank Mauro Giacca for helpful discussions.

REFERENCES

1. Baldwin AS, Jr. The NF-κB and IκB proteins: new discoveries and insights. Annu Rev Immunol 1996;14:649–683.
2. Grilli M, Memo M. Nuclear factor-κB/Rel proteins: a point of convergence of signalling pathways relevant in neuronal function and dysfunction. Biochem Pharmacol 1999;57:1–7.
3. O'Neill LA, Kaltschmidt C. NF-κB: a crucial transcription factor for glial and neuronal cell function. Trends Neurosci 1997;20:252–258.
4. Chen FE, Ghosh G. Regulation of DNA binding by Rel/NF-κB transcription factors: structural views. Oncogene 1999;18:6845–6852.
5. Ghosh S, May MJ, Kopp EB. NF-κB and Rel proteins: evolutionarily conserved mediators of immune responses. Annu Rev Immunol 1998;16:225–260.
6. Kiernan R, Bres V, Ng RW, Coudart MP, El Messaoudi S, Sardet C, Jin DY, Emiliani S, Benkirane M. Post-activation turn-off of NF-κB-dependent transcription is regulated by acetylation of p65. J Biol Chem 2003;278:2758–2766.
7. Rayet B, Gelinas C. Aberrant rel/nfkb genes and activity in human cancer. Oncogene 1999;18:6938–6947.
8. Cahir McFarland ED, Izumi KM, Mosialos G. Epstein-barr virus transformation: involvement of latent membrane protein 1-mediated activation of NF-κB. Oncogene 1999;18:6959–6964.
9. Kucharczak J, Simmons MJ, Fan Y, Gelinas C. To be, or not to be: NF-κB is the answer - role of Rel/NF-κB in the regulation of apoptosis. Oncogene 2003;22:8961–8982.
10. Inoue J, Gohda J, Akiyama T, Semba K. NF-κB activation in development and progression of cancer. Cancer Sci 2007;98:268–274.
11. Ito K. Impact of post-translational modifications of proteins on the inflammatory process. Biochem Soc Trans 2007;35:281–283.
12. Mohamed MR, McFadden G. NFκB inhibitors: strategies from poxviruses. Cell Cycle 2009;8:3125–3132.
13. Perkins ND. The Rel/NF-κB family: friend and foe. Trends Biochem Sci 2000;25:434–440.
14. Magné N, Toillon RA, Bottero V, Didelot C, Houtte PV, Gerard JP, Peyron JF. NF-κB modulation and ionizing radiation: mechanisms and future directions for cancer treatment. Cancer Lett 2006;231:158–168.
15. Namba H, Saenko V, Yamashita S. Nuclear factor-kB in thyroid carcinogenesis and progression: a novel therapeutic target for advanced thyroid cancer. Arq Bras Endocrinol Metabol 2007;51:843–851.
16. Cilloni D, Martinelli G, Messa F, Baccarani M, Saglio G. Nuclear factor kB as a target for new drug development in myeloid malignancies. Haematologica 2007;92:1224–1229.
17. Chen LF, Fischle W, Verdin E, Greene WC. Duration of nuclear NF-κB action regulated by reversible acetylation. Science 2001;293:1653–1657.
18. Chen LF, Mu Y, Greene WC. Acetylation of RelA at discrete sites regulates distinct nuclear functions of NF-κB. EMBO J 2002;21:6539–6548.
19. Sheppard KA, Rose DW, Haque ZK, Kurokawa R, McInerney E, Westin S, Thanos D, Rosenfeld MG, Glass CK, Collins T. Transcriptional activation by NF-κB requires multiple coactivators. Mol Cell Biol 1999;19:6367–6378.
20. Vanden Berghe W, De BK, Boone E, Plaisance S, Haegeman G. The nuclear factor-κB engages CBP/p300 and histone acetyltransferase activity for transcriptional activation of the interleukin-6 gene promoter. J Biol Chem 1999;274:32091–32098.
21. Roth SY, Denu JM, Allis CD. Histone acetyltransferases. Annu Rev Biochem 2001;70:81–120.
22. Furia B, Deng L, Wu K, Baylor S, Kehn K, Li H, Donnelly R, Coleman T, Kashanchi F. Enhancement of nuclear factor-κB acetylation by coactivator p300 and HIV-1 Tat proteins. J Biol Chem 2002;277:4973–4980.
23. Chen LF, Greene WC. Regulation of distinct biological activities of the NF-κB transcription factor complex by acetylation. J Mol Med 2003;81:549–557.
24. Deng WG, Zhu Y, Wu KK. Up-regulation of p300 binding and p50 acetylation in tumor necrosis factor-α-induced cyclooxygenase-2 promoter activation. J Biol Chem 2003;278:4770–4777.
25. Schmitz ML, Mattioli I, Buss H, Kracht M. NF-κB: a multifaceted transcription factor regulated at several levels. ChemBioChem 2004;5:1348–1358.
26. Quivy V, Van Lint C. Regulation at multiple levels of NF-κB-mediated transactivation by protein acetylation. Biochem Pharmacol 2004;68:1221–1229.
27. Chen LF, Greene WC. Shaping the nuclear action of NF-κB. Nat Rev Mol Cell Biol 2004;5:392–401.
28. Chen FE, Huang DB, Chen YQ, Ghosh G. Crystal structure of p50/p65 heterodimer of transcription factor NF-κB bound to DNA. Nature 1998;391:410–413.
29. Jorgensen WL, Chandrasekhar J, Madura JD, Impey RW, Klein ML. Comparison of simple potential functions for simulating liquid water. J Chem Phys 1983;79:926–935.
30. Wang J, Cieplak P, Kollman PA. How well does a restrained electrostatic potential (RESP) model perform in calculating conformational energies of organic and biological molecules? J Comput Chem 2000;21:1049–1074.
31. Ponder JW, Case DA. Force fields for protein simulations. Adv Protein Chem 2003;66:27–85.
32. Bayly CI, Cieplak P, Cornell WD, Kollman PA. A well-behaved electrostatic potential based method using charge restraints for deriving atomic charges: the RESP model. J Phys Chem 1993;97:10269–10280.
33. Berendsen HJC, van der Spoel D, van Drunen R. GROMACS:a message-passing parallel molecular dynamics implementation. Comp Phys Commun 1995;91:43–56.
34. Lindhal E, Hess B, van der Spoel D. GROMACS 3.0: a package for molecular simulation and trajectory analysis. J Mol Mod 2001;7:306–317.
35. Humphrey W, Dalke A, Schulten K. VMD: visual molecular dynamics. J Mol Graph 1996;14:33–38.
36. Lavery R, Sklenar H. Defining the structure of irregular nucleic acids: conventions and principles. J Biomol Struct Dyn 1989;6:655–667.
37. Anselmi C, De Santis P, Paparcone R, Savino M, Scipioni A. From the sequence to the superstructural properties of DNAs. Biophys Chem 2002;95:23–47.
38. Olson WK, Bansal M, Burley SK, Dickerson RE, Gerstein M, Harvey SC, Heinemann U, Lu XJ, Neidle S, Shakked Z, Sklenar H, Suzuki M, Tung CS, Westhof E, Wolberger C, Berman HM. A

standard reference frame for the description of nucleic acid base-pair geometry. J Mol Biol 2001;313:229–237.
39. Baker NA, Sept D, Joseph S, Holst MJ, McCammon JA. Electrostatics of nanosystems: application to microtubules and the ribosome. Proc Natl Acad Sci U S A 2001;98:10037–10041.
40. Kollman PA, Massova I, Reyes C, Kuhn B, Huo S, Chong L, Lee M, Lee T, Duan Y, Wang W, Donini O, Cieplak P, Srinivasan J, Case DA, Cheatham TE, III. Calculating structures and free energies of complex molecules: combining molecular mechanics and continuum models. Acc Chem Res 2000;33:889–897.
41. Case DA, Darden TA, Cheatham TE, III, Simmerling CL, Wang J, Duke RE, Luo R, Walker RC, Zhang W, Merz KM, Roberts BP, Wang B, Hayik S, Roitberg A, Seabra G, Kolossvai I, Wong KF, Paesani F, Vanicek J, Liu J, Wu X, Brozell SR, Steinbrecher T, Gohlke H, Cai Q, Ye X, Wang J, Hsieh M-J, Cui G, Roe DR, Mathews DH, Seetin MG, Sagui C, Babin V, Luchko T, Gusarov S, Kovalenko A, Kollman PA. AMBER 11. In. San Francisco: University of California; 2010.
42. Hartmann B, Piazzola D, Lavery R. BI-BII transitions in B-DNA. Nucleic Acids Res 1993;21:561–568.
43. Falvo JV, Thanos D, Maniatis T. Reversal of intrinsic DNA bends in the IFN β gene enhancer by transcription factors and the architectural protein HMG I(Y). Cell 1995;83:1101–1111.
44. Perez A, Marchan I, Svozil D, Sponer J, Cheatham TE, III, Laughton CA, Orozco M. Refinement of the AMBER force field for nucleic acids: improving the description of alpha/gamma conformers. Biophys J 2007;92:3817–3829.
45. Schlitter J. Estimation of absolute and relative entropies of macromolecules using the covariance-matrix. Chem Phys Lett 1993;215: 617–621.